Optical properties of fully amorphous silicon

Sadao Adachi and Hirofumi Mori
Department of Electronic Engineering, Faculty of Engineering, Gunma University, Kiryu-shi, Gunma 376-8515, Japan
(Received 18 February 2000)

We have determined the complex dielectric function, $\varepsilon(E)=\varepsilon_1(E)+i\varepsilon_2(E)$, for self-implanted amorphous silicon (*a*-Si) by spectroscopic ellipsometry (SE) in the 1.5–5.2-eV photon-energy range at room temperature. The measured SE spectra show a single broad peak in $\varepsilon_2(\sim 26.6)$ at $E\sim 3.45$ eV, which is typically observed in amorphous tetrahedral semiconductors. The SE $\varepsilon(E)$ data, together with the literature data which exhibit the largest peak in $\varepsilon_2(\sim 30)$ at $E\sim 3.7$ eV and have been widely used as a reference of ''dense'' *a*-Si, are analyzed by means of the Bruggeman effective-medium approximation. The results clearly indicate that the self-implanted *a*-Si sample is in the fully amorphous state, while the literature data contain microcrystalline component (μc-Si) in its spectra. The volume fraction of μc-Si is estimated to be about 53%. The optical spectra of μc-Si are found to be quite different from those of single-crystalline silicon, especially in the vicinity of the sharp critical-point features. The SE $\varepsilon(E)$ data of the self-implanted *a*-Si are successfully parametrized using Jellison-Modine's dispersion expression.

I. INTRODUCTION

There has been considerable interest in amorphous semiconductors because they have a number of interesting physical properties as well as numerous potential applications. It is well known that knowledge of the refractive index and absorption coefficient of amorphous semiconductors is of great importance in the design and analysis of various optoelectronic devices. Experimental data on the optical constants as a function of photon energy are available at the present time for a number of amorphous semiconductors.[1]

Optical properties of amorphous silicon (*a*-Si) are known to strongly depend on preparation techniques and conditions. Structural studies suggested that *a*-Si films contain microvoids on the order of 0.5–1.0 nm.[2] These structural defects give rise to a large density of states in the gap of the semiconductor.

Although it is generally accepted that the best characterized amorphous state can be formed by ion implantation, this state is not unique.[3] The ion-implanted, unrelaxed *a*-Si releases substantial enthalpy during low-temperature annealing toward a relaxed configuration.[4] It was reported[3] that self-implanted *a*-Si layer, regardless of relaxed or unrelaxed state, is about 2% less dense than crystalline silicon (*c*-Si). Fried *et al.*[5,6] have shown that spectroscopic-ellipsometry (SE) data of as-implanted, unrelaxed *a*-Si differ from those of implanted, relaxed (annealed) sample. More recently, Lee, Kim, and Oh[7] have investigated an importance of the choice of sample (unrelaxed or relaxed) as a reference in analyzing SE spectra of ion-implanted *a*-Si. These authors, however, did not completely rule out the origin of difference in optical properties between the unrelaxed and relaxed amorphous samples.[5–7]

The purpose of this paper is twofold: (i) to report the optical constants of self-implanted *a*-Si measured by SE and (ii) to analyze these data and the literature data widely used as a reference of ''dense'' *a*-Si (Refs. 8 and 9) based on the Bruggeman effective-medium approximation (EMA; Ref. 10). The literature data give a maximum value of $\varepsilon_2\sim 30$ near $E\sim 3.7$ eV. This value is considerably larger than the value of $\varepsilon_2\sim 26.6$ at $E\sim 3.45$ obtained in this present study. The dielectric function exhibiting the largest ε_2 at its peak is believed to be most representative of a bulk dense sample.[9] It is, however, shown here that the literature data contain microcrystalline component (μc-Si) in its spectra. It should be noted that the literature data were obtained from a sample deposited by low-pressure chemical-vapor-deposition (LPCVD) technique at 571 °C on thermally oxidized *c*-Si wafer.

II. EXPERIMENT

The samples used in this study were *p*-type Si(100) with resistivity of about 30 Ω cm. Samples were implanted with singly charged Si ions at an energy of 150 keV and a dose of $2\times 10^{15}\,\mathrm{cm}^{-2}$ at room temperature. No thermal annealing was performed.

Surface morphology of the self-implanted Si(100) sample was checked by means of an *ex situ* atomic force microscopy (AFM), using a Digital Instruments Nanoscope III. The AFM image was acquired in the tapping mode and in the repulsive force regime with a force constant of the order of 1 nN between the AFM tip and sample surface.

The automatic SE instrument used was of the rotating analyzer type (DVA-36VW-A, Mizojiri Optical, Co., Ltd.). A 150-W xenon lamp was used as the light source. SE measurements were carried out ellipsometry in the 1.5–5.2-eV photon-energy range at room temperature after cleaning the sample surface with organic solvents and then rinsing in a 1.5% aqueous HF solution to remove the native oxide layer.

III. RESULTS AND DISCUSSION

A. AFM observation

We used *ex situ* AFM to evaluate surface morphology of self-implanted *a*-Si sample. Figure 1 shows a large-scale ($1\times 1\,\mu\mathrm{m}^2$) AFM image for the self-implanted *a*-Si sample. The image clearly demonstrates that the Si-ion-implanted sample has a shiny flat surface. The root-mean-square (rms)

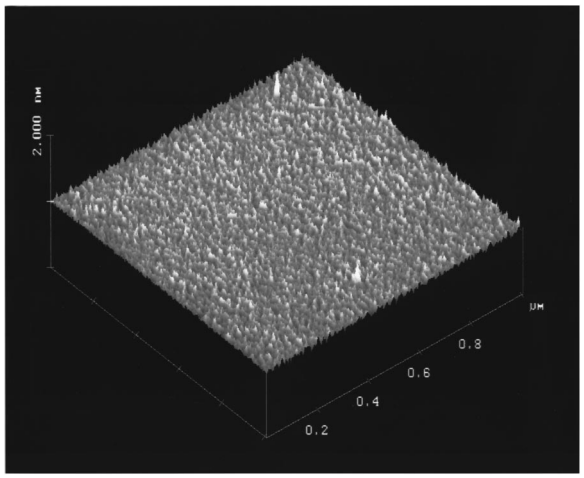

FIG. 1. Large-scale ($1\times1\ \mu m^2$) AFM image for self-implanted *a*-Si sample (x,y:0.2 μm/div;z:2 nm/div). The root-mean-square (rms) roughness obtained from this image is ~0.20 nm.

roughness obtained from this image is ~0.20 nm. We find that this value is comparable to those for polished, HF-etched Si(111) wafers measured by scanning tunneling microscopy (0.12–0.18 nm; Ref. 11). Notice that not only oxide overlayer but also surface microroughness have effects upon the ellipsometric data.[12] We, however, consider that the present sample will give the true bulk dielectric function of *a*-Si. This is because it has nearly flat sample surface, as has been demonstrated by AFM.

B. SE results

Figure 2 shows the pseudodielectric-function spectra, $\varepsilon(E)=\varepsilon_1(E)+i\varepsilon_2(E)$, for self-implanted *a*-Si sample measured by SE (solid circles). The pseudodielectric function is a quantity derived from SE by means of a two-phase (ambient/sample) model.[13] It is, thus, exactly equal to the true dielectric function of a given sample if its surface is perfectly abrupt and film-free. For comparison, the $\varepsilon(E)$ spectra for LP-CVD *a*-Si measured by Bagley *et al.*[8,9] are shown in Fig. 2 by the open circles. These data have been popularly used as a reference of dense *a*-Si in many optical analyses of processed silicon samples.[14–22]

A single broad peak found in the $\varepsilon_2(E)$ spectrum [Fig. 2(b)] is typically observed in amorphous tetrahedral semiconductors.[1] The main spectral difference between these two samples is that the ε_2 peak in the self-implanted *a*-Si occurs at a considerably lower energy than that in the LP-CVD *a*-Si sample. The experimental data of the self-implanted *a*-Si give a maximum value of $\varepsilon_2\sim26.6$ near $E\sim3.45$ eV, while a value of $\varepsilon_2\sim30$ at $E\sim3.7$ eV was obtained from the LP-CVD sample. It is generally believed that the dielectric function exhibiting the largest ε_2 value at its peak is most representative of the bulk dense sample. The ε_2 value of ~30 has been shown to be an apparently limiting peak value for *a*-Si, and thus its $\varepsilon(E)$ spectra have long been regarded as the ''intrinsic'' dielectric properties of *a*-Si. Similar values have also been obtained by glow discharge,[23,24] multipole plasma deposition,[25] plasma-enhanced CVD,[26] and LP-CVD techniques.[27] In the following, however, it is shown that this is not true, i.e., such a larger ε_2 sample is not in the full amorphous state.

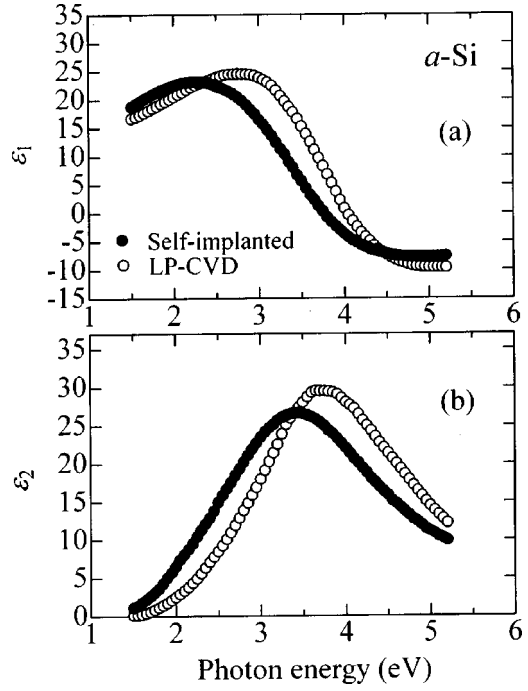

FIG. 2. Pseudodielectric-function spectra, $\varepsilon(E)=\epsilon_1(E)+i\varepsilon_2(E)$, for self-implanted *a*-Si measured by SE (solid circles). The $\varepsilon(E)$ spectra for LP-CVD *a*-Si reported by Bagley *et al.* (Refs. 8 and 9) are also shown by the open circles.

C. Bruggeman EMA analysis

In order to give more detailed information on the spectral difference seen in Fig. 2, we carried out the EMA in which an amorphous layer is assumed as a physical mixture of fully amorphous silicon (*a*-Si; ε_a) and μc-Si ($\varepsilon_{\mu c}$). Here we used the Bruggeman EMA.[10] The Bruggeman EMA can now be defined by the following two expressions:

$$f_a\frac{\varepsilon_a-\varepsilon}{\varepsilon_a+2\varepsilon}+f_{\mu c}\frac{\varepsilon_{\mu c}-\varepsilon}{\varepsilon_{\mu c}+2\varepsilon}=0, \tag{1}$$

$$f_a+f_{\mu c}=1, \tag{2}$$

where f_i and ε_i are, respectively, the volume fraction and complex dielectric function of each of the components *i*, and ε is the complex dielectric function of the material studied.

The two-phase model was used in the present analysis. The unknown parameters were numerically determined by minimizing the following mean squares deviation with a regression program [linear regression analysis (LRA)]:[13]

$$\sigma^2=\frac{1}{N-P-1}\sum_{j=1}^{N}\{(\tan\Psi_j^{\exp}-\tan\Psi_j^{\mathrm{calc}})^2+(\cos\Delta_j^{\exp}-\cos\Delta_j^{\mathrm{calc}})^2\}, \tag{3}$$

where N is the number of data points and P is the number of unknown model parameters. Here Ψ and Δ are the ratio of amplitudes and the difference in phase of reflectance for *s*- and *p*-polarized states, respectively. The best-fit model is selected as that yielding a minimum value of unbiased estimator σ.

The $\varepsilon(E)$ data of the LP-CVD *a*-Si are used as a reference (i.e., ε_a) in the simulation of the self-implanted *a*-Si

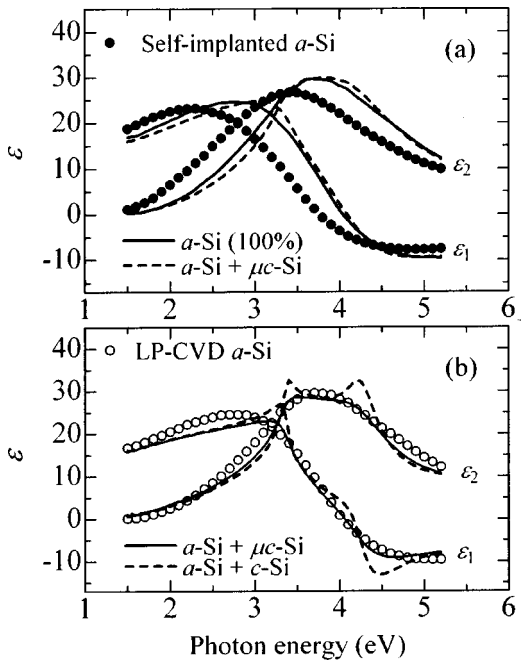

FIG. 3. Bruggeman EMA-LRA results for self-implanted and LP-CVD *a*-Si samples. A physical mixture of *a*-Si and μc-Si (or *c*-Si) is assumed in the Brugemann EMA. The LP-CVD *a*-Si data (Refs. 8 and 9) are used as a reference (ε_a) in the simulation of the self-implanted *a*-Si data in (a), and vice versa in (b). The structural parameters and unbiased estimators σ obtained from these analyses are listed in Table I.

data, and vice versa. The results of this simulation are shown in Fig. 3. The structural parameters and unbiased estimators obtained from this simulation are summarized in Table I.

The μc-Si $\varepsilon(E)$ spectra used in the LRA-EMA analysis are obtained by calculating the model dielectric function (MDF) in Refs. 12, 28, and 29. Here we assume that each critical point (CP) in μc-Si has the same strength parameter value as that of *c*-Si. This assumption is consistent with the requirement of an oscillator-strength sum rule in crystalline solids.[30] We, however, consider that the broadening parameters in μc-Si are not the same as those in *c*-Si. As we will see next, the resultant μc-Si $\varepsilon(E)$ spectra differ appreciably from those of *c*-Si, especially in the vicinity of the sharp CP features.

TABLE I. Bruggeman EMA-LRA parameters obtained from the two-phase model.

Sample	f_a (%)	$f_{\mu c}$ (%)	σ
Self-implanted *a*-Si[a]	100		0.0618
Self-implanted *a*-Si[b]	75	25	0.0703
LP-CVD *a*-Si[c]	46.9	53.1	0.0248
LP-CVD *a*-Si[d]	46.9	53.1 (f_c)	0.0349

[a]Assumed as 100% *a*-Si (LP-CVD *a*-Si) [solid lines; Fig. 3(a)].
[b]Assumed as a mixture of 75% *a*-Si (LP-CVD *a*-Si) and 25% μc-Si [dashed lines; Fig. 3(a)].
[c]Assumed as a mixture of *a*-Si (self-implanted *a*-Si) and μc-Si [solid lines; Fig. 3(b)].
[d]Assumed as a mixture of *a*-Si (self-implanted *a*-Si) and *c*-Si [dashed lines; Fig. 3(b)].

As seen in Fig. 3(a), the use of the LP-CVD $\varepsilon(E)$ data as a reference of fully amorphous silicon gives no good simulated results. The best-fit result, in this case, can be achieved by putting $f_a = 100\%$ (i.e., neglecting μc-Si component). The corresponding σ value is 0.0618 (solid lines). This value is considerably smaller than that of $(f_a, f_{\mu c}) = (75\%, 25\%)$ (dashed lines). It is found that larger $f_{\mu c}$ value results in larger σ (i.e., poorer fit).

The entirely opposite assumption, i.e., regarding the self-implanted *a*-Si as a fully amorphous material, resulted in reasonable agreement with the LP-CVD *a*-Si data, as shown in Fig. 3(b) by the solid lines. It may, thus, be considered that the LP-CVD *a*-Si sample (Refs. 8 and 9) is in the amorphous-crystal intermediate state, not in the fully amorphous state. Notice that the LP-CVD *a*-Si sample was deposited at moderately high temperature 571 °C. The $\varepsilon_2(E)$ data reported in Refs. 23–27 also show larger ε_2 values ($\sim$30) near $E \sim 3.7$ eV. These samples were also deposited at moderately high temperatures ($\geqslant$250 °C).

Fried *et al.*[5,6] studied the optical properties of different kinds of amorphous silicon prepared by self-ion implantation and subsequent thermal annealing (500 °C, 3h) and found that the complex dielectric function of the unrelaxed *a*-Si differs from that of the annealed, relaxed *a*-Si. They also found that the $\varepsilon(E)$ spectra of the LP-CVD *a*-Si (Refs. 8 and 9) are very close to those of the annealed, relaxed *a*-Si.

The dashed lines in Fig. 3(b) show the simulated results using *c*-Si $\varepsilon(E)$ data (Ref. 31) instead of μc-Si data. It is evident that the use of the *c*-Si $\varepsilon(E)$ data provides no good simulated result (see also Table I).

D. $\varepsilon(E)$ spectra of μc-Si

Figure 4 shows the MDF-calculated $\varepsilon(E)$ spectra for μc-Si deduced from the Bruggeman EMA-LRA result (heavy solid lines). The MDF CP parameters used in the calculation are listed in Table II. The $\varepsilon(E)$ data of *c*-Si are also plotted by the light solid lines. These data were taken from Ref. 31. It is clear from Fig. 4 that the μc-Si $\varepsilon(E)$ spectra differ largely from the *c*-Si spectra.

The dielectric function in the interband transition region of crystalline and microcrystalline semiconductors depends fundamentally on the electronic energy-band structure of the semiconductors.[12] The relation between the electronic energy-band structure and $\varepsilon_2(E)$ can be given by

$$\varepsilon_2(E) = \frac{4e^2\hbar^2}{\pi\mu^2 E^2} \int dk |P_{cv}(k)|^2 \delta[E_c(k) - E_v(k) - E], \tag{4}$$

where μ is the combined density-of-states mass, the Dirac δ function represents the joint spectral density of states between the valence-band $[E_v(k)]$ and conduction-band states $[E_c(k)]$ differing by the energy $E = \hbar\omega$ of the incident light, $P_{cv}(k)$ is the momentum matrix element between the valence-band and conduction-band states, and the integration is performed over the first Brillouin zone.

In the MDF, Eq. (4) can be written as[12,28,29]

$$\varepsilon_2(E) = \sum_{s=1}^{M} \frac{4e^2\hbar^2}{\pi(\mu^s)^2 E^2} |P_{cv}^s(E)|^2 J_{cv}^s(E), \tag{5}$$

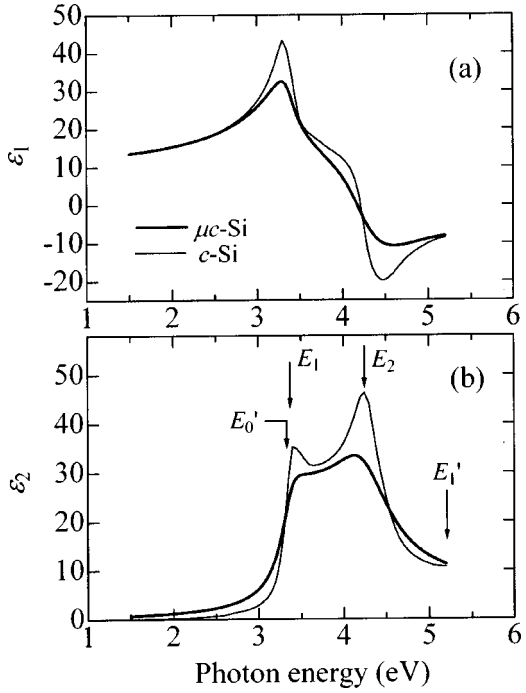

FIG. 4. MDF-calculated $\varepsilon(E)$ spectra for μc-Si deduced from the Bruggeman EMA-LRA result (heavy solid lines). The MDF parameters used in this calculation are listed in Table II. The experimental $\varepsilon(E)$ spectra for c-Si (Ref. 31) are also shown by the light solid lines. The vertical arrows indicate the positions of each CP.

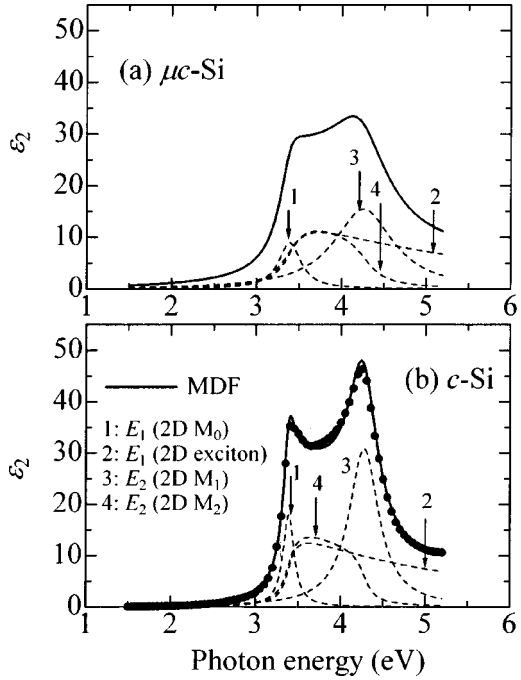

FIG. 5. MDF-calculated $\varepsilon_2(E)$ spectra for (a) μc-Si and (b) c-Si (solid lines). The MDF parameters used in these calculations are listed in Table II. The experimental $\varepsilon_2(E)$ spectrum for c-Si taken from Ref. 31 is also shown in (b) by the solid circles. The dashed lines represent individual contributions to ε_2 of the E_1 and E_2 gaps. They are obtained from Eqs. (8) [two-dimensional (2D) M_0 CP] and (10) (2D exciton) for the E_1-gap contributions and from Eqs. (12) (2D-M_1 CP) and (14) (2D-M_2 CP) for the E_2-gap contributions (Ref. 29).

where $J^s_{cv}(E)$ is the joint density-of-states function of the sth interband CP. The joint density-of-states function $J^s_{cv}(E)$ mainly determines the interband contribution to $\varepsilon_2(E)$ and thus to the optical constants of solids.

We show in Figs. 5(a) and 5(b) the MDF-calculated $\varepsilon_2(E)$ spectra for μc-Si and c-Si, respectively. The MDF CP parameters used in these calculations are listed in Table II. The experimental $\varepsilon_2(E)$ spectrum of c-Si (Ref. 31) is also shown in Fig. 5(b) by the solid circles. We can understand from Fig. 5(b) that our MDF calculation shows excellent agreement with the experimental $\varepsilon_2(E)$ data of c-Si over the entire range of photon energies.

TABLE II. MDF parameters for μc-Si obtained from the Bruggeman EMA-LRA. Values for c-Si are shown in parentheses.

Parameter	μc-Si (c-Si)
E_0' (eV)	3.35
C	0.07
γ	0.18 (0.09)
E_1 (eV)	3.39
B_1	5.22
B_{1x} (eV)	1.44
Γ (eV)	0.16 (0.08)
E_2 (eV)	4.28
C	3.08
γ	0.20 (0.10)
F	3.82
Γ (eV)	0.20 (0.10)
E_1' (eV)	5.33
C	0.30
γ	0.24 (0.12)
$\varepsilon_{1\infty}$	0.40 (0.40)

The prominent CP features seen in the $\varepsilon(E)$ spectra of μc-Si and c-Si are the E_1 and E_2 structures at $E\sim3.4$ and ~4.3 eV, respectively. The disappearance of the peculiar CP features in amorphous material (Fig. 2) is due to the breakdown of crystal periodicity in the amorphous material. As shown in Fig. 4, the $\varepsilon(E)$ spectra of μc-Si are quite different from those of c-Si. This difference can be successfully explained by changing the Γ values between μc-Si and c-Si (see Table II). This fact is not surprising since microcrystalline material has an additional lifetime broadening mechanism caused by the grain boundaries.

We have already shown[32] that the Γ values in amorphous materials are considerably larger than those of the interband transitions in crystalline materials. It is important to note that the amorphous materials preserve the short-range order, in this case the tetrahedral coordination, but do not preserve the long-range order. Therefore, it can be considered that the large Γ values required in the amorphous materials are due to the effects of long-range disorder (and short-range defects) in these materials.[32] If the main broadening mechanism in μc-Si is due to such structural defects, the Γ value may be strongly dependent on its crystalline quality or, strictly speaking, grain size. Indeed, we have found that the Γ's in self-implanted silicon have strong dependence on Si-ion dose and increase with increasing it.[33]

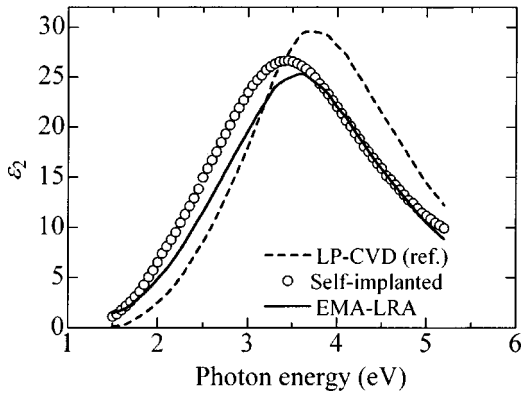

FIG. 6. Bruggeman EMA-LRA results for self-implanted *a*-Si sample (solid line). The experimental $\varepsilon_2(E)$ data for self-implanted *a*-Si sample are plotted by the solid circles. The Bruggeman effective medium in this case deals with the overlayer consisting of two constituents, voids and bulk amorphous silicon (*a*-Si). The LP-CVD *a*-Si data, shown by the dashed line, are used as a reference in this analysis.

If the LP-CVD *a*-Si data indeed have a microcrystalline component, then they should show some evidence of the E_1 and E_2 transitions of the crystalline material. However, we cannot clearly recognize such a feature in the corresponding spectra. Only the plateau can be recognized in the 3.5–4-eV region of the $\varepsilon_2(E)$ spectrum (Fig. 2). It should be noted that such a plateau has been typically observed in the $\varepsilon_2(E)$ spectra of microcrystalline samples (e.g., Refs. 21, 34–36). In these studies, the microcrystalline nature was independently checked by dark conductivity and Raman scattering measurements.[34,35] In particular, all the μc-Si Raman spectra displayed a peak near 520 cm^{-1}, characteristic of a crystalline phase. As we can see in Fig. 2, no plateaulike feature can be found in the $\varepsilon_2(E)$ spectrum of the self-implanted *a*-Si sample. We have also measured Raman spectra on this sample, but not observed a peak related to the crystalline phase.

A decrease of the peak height in $\varepsilon_2(E)$ accompanied by a shift of its peak to lower energies is a characteristic behavior of microscopically rough surface. In order to account for the effect of rough surface, we performed the Bruggeman EMA-LRA analysis assuming a three-phase model (ambient/roughened *a*-Si overlayer/bulk *a*-Si). The Bruggeman effective medium in this case deals with the overlayer consisting of two constituents, voids (density deficit; $\varepsilon_v = 1 + i0$) and bulk amorphous silicon (a-Si;ε_a), where the LP-CVD *a*-Si data are used as a reference (i.e., ε_a).

Figure 6 shows the best-fit results of this simulation. The open circles represent the self-implanted *a*-Si data. The analysis yields a roughened overlayer thickness of $d = 3.4$ nm with a void fraction of $f_v \sim 31\%$. As expected, the simulated $\varepsilon_2(E)$ spectrum indicates a decrease of the peak height accompanied by a shift of its peak to lower energy. However, it is evident that this spectrum shows no good agreement with the experimental data (open circles). From this fact, we can conclude that the self-implanted *a*-Si sample contains no or only a very small number of void networks, as independently confirmed by the AFM observation (i.e., very flat surface, see Sec. III A).

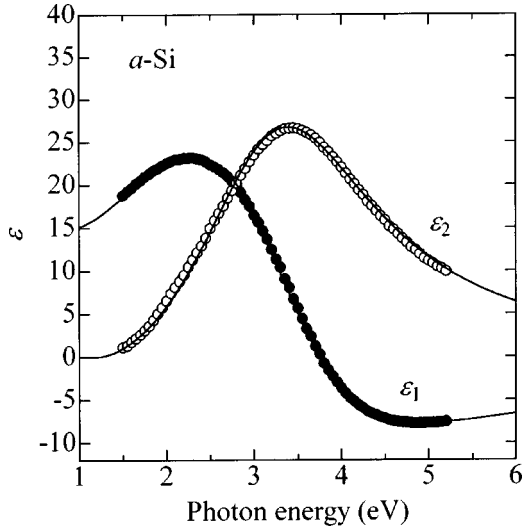

FIG. 7. $\varepsilon(E)$ spectra for self-implanted *a*-Si. The solid and open circles represent the experimental SE data. The solid lines show the calculated spectra from Eqs. (6) and (7). The model parameters obtained from these fits are listed in Table III.

E. Parametrization of *a*-Si $\varepsilon(E)$ data

It is of both technical and scientific interest to obtain the analytical expression of the optical constants of semiconductors. Assuming the parabolic valence and conduction bands and the **k**-independent momentum-matrix element, Jellison and Modine[37] proposed a new parametrization of $\varepsilon(E)$ for amorphous semiconductors. An expression for $\varepsilon_2(E)$ obtained by them can be written as[37]

$$\varepsilon_2(E) = \begin{cases} 0 & E \leqslant E_g \\ \dfrac{AE_0C(E-E_g)^2}{(E^2-E_0^2)^2+C^2E^2}\dfrac{1}{E} & E > E_g, \end{cases} \tag{6}$$

where E_g, E_0, A, and C are in units of energy.

The corresponding Kramers-Kronig transformation gives[37]

$$\begin{aligned} \varepsilon_1(E) = {} & \frac{AC}{\pi\zeta^4}\frac{a_{\ln}}{2\alpha E_0}\ln\left(\frac{E_0^2+E_g^2+\alpha E_g}{E_0^2+E_g^2-\alpha E_g}\right) - \frac{A}{\pi\zeta^4}\frac{a_{\arctan}}{E_0} \\ & \times\left[\pi - \arctan\left(\frac{2E_g+\alpha}{C}\right) + \arctan\left(\frac{-2E_g+\alpha}{C}\right)\right] \\ & + 2\frac{AE_0}{\pi\zeta^4\alpha}E_g(E^2-\gamma^2)\left[\pi + 2\arctan\left(2\frac{\gamma^2-E_g^2}{\alpha C}\right)\right] \\ & - \frac{AE_0C}{\pi\zeta^4}\frac{E^2+E_g^2}{E}\ln\left(\frac{|E-E_g|}{E+E_g}\right) \\ & + 2\frac{AE_0C}{\pi\zeta^4}E_g\ln\left[\frac{|E-E_g|(E+E_g)}{\sqrt{(E_0^2-E_g^2)^2+E_g^2C^2}}\right] + \varepsilon_1(\infty), \end{aligned} \tag{7}$$

where $a_{\ln}$, $a_{\arctan}$, ζ, α, and γ are defined in Ref. 37.

The solid lines in Fig. 7 represent the calculated results of Eqs. (6) and (7). Table III lists the fit-determined parameter values. Excellent agreement can be achieved between the

TABLE III. Model parameters used in Eqs. (5) and (6) for fully amorphous silicon (*a*-Si).

Parameter	Value
E_g (eV)	1.11
A (eV)	150
E_0 (eV)	3.40
C (eV)	2.55
$\varepsilon_1(\infty)$	0.17

calculation and experiment over the entire range of photon energies. This result greatly encourages the use of the self-implanted *a*-Si $\varepsilon(E)$ data as a reference of fully amorphous silicon.

IV. CONCLUSIONS

Using SE in the 1.5–5.2-eV photon-energy range, we have determined the complex dielectric function, $\varepsilon(E) = \varepsilon_1(E) + i\varepsilon_2(E)$, of *a*-Si fabricated by self-ion implantation at an energy of 150 keV and a dose of $2\times10^{15}\,\mathrm{cm}^{-2}$. The measured $\varepsilon(E)$ spectra show a single broad peak in ε_2 ($\sim$26.6) at $E\sim3.45$ eV, which is typically observed in amorphous tetrahedral semiconductors. The present $\varepsilon(E)$ data, together with the literature data which exhibit the largest peak in ε_2 ($\sim$30) at $E\sim3.75$ eV and have been widely used as a reference of dense *a*-Si, are investigated by means of the Bruggeman EMA-LRA simulation. The results clearly suggest that the self-implanted *a*-Si sample is in the fully amorphous state, while the dense *a*-Si corresponds to those containing μc-Si component in its substance. The volume fraction of μc-Si is estimated to be $\sim$53%. The optical spectra of μc-Si are quite different from those of *c*-Si, especially in the vicinity of the sharp CP features. An *ex situ* AFM image confirms that the self-implanted *a*-Si surface is very flat, rms roughness of $\sim$0.20 nm. The fact promises that the optical data for the self-implanted *a*-Si can be used as a reference of fully amorphous silicon. For the sake of convenience, the $\varepsilon(E)$ data of the self-implanted *a*-Si are successfully parametrized using Jellison-Morine's model.

ACKNOWLEDGMENTS

The authors wish to thank Dr. M. Takahashi of NTT Telecommunications Energy Laboratories for Si-ion implantations. The authors also wish to thank Dr. T. Miyazaki and Dr. S. Ozaki for useful discussion. This work was supported in part by the Gunma University–Satellite Venture Business Laboratory (GU-SVBL).

[1] S. Adachi, *Optical Constants in Crystalline and Amorphous Semiconductors: Numerical Data and Graphical Information* (Kluwer Academic, Boston, 1999).
[2] R. J. Temkin, W. Paul, and G. A. N. Connell, Adv. Phys. **22**, 581 (1973).
[3] J. S. Custer, M. O. Thompson, D. C. Jacobson, J. M. Poate, S. Roorda, W. C. Sinke, and F. Spaepen, Appl. Phys. Lett. **64**, 437 (1994).
[4] S. Roorda, W. C. Sinke, J. M. Poate, D. C. Jacobson, S. Dierker, B. S. Dennis, D. J. Eaglesham, F. Spaepen, and P. Fuoss, Phys. Rev. B **44**, 3702 (1991).
[5] M. Fried, T. Lohner, W. A. M. Aarnink, L. S. Hanekamp, and A. van Silfhout, J. Appl. Phys. **71**, 5260 (1992).
[6] M. Fried and A. van Silfhout, Phys. Rev. B **49**, 5699 (1994).
[7] S. Lee, S. Y. Kim, and S. Oh, Jpn. J. Appl. Phys., Part 1 **35**, 5929 (1996).
[8] B. G. Bagley, D. E. Aspnes, G. K. Celler, and A. C. Adams, in *Laser and Electron-Beam Interactions with Solids*, edited by B. R. Appleton and G. K. Celler (Elsevier, New York, 1982), p. 483.
[9] D. E. Aspnes, A. A. Studna, and E. Kinsbron, Phys. Rev. B **29**, 768 (1984).
[10] M. Erman, J. B. Theeten, P. Chambon, S. M. Kelso, and D. E. Aspnes, J. Appl. Phys. **56**, 2664 (1984).
[11] E. Hartmann, P. O. Hahn, and R. J. Behm, J. Appl. Phys. **69**, 4273 (1991).
[12] S. Adachi, *Optical Properties in Crystalline and Amorphous Semiconductors: Materials and Fundamental Principles* (Kluwer Academic, Boston, 1999).
[13] R. M. A. Azzam and N. M. Bashara, *Ellipsometry and Polarized Light* (North-Holland, Amsterdam, 1977).
[14] R. W. Collins, A. H. Clark, S. Guha, and C.-Y. Huang, J. Appl. Phys. **57**, 4566 (1985).
[15] K. Vedam, P. J. McMarr, and J. Narayan, Appl. Phys. Lett. **47**, 339 (1985).
[16] T. V. Herak, J. J. Schellenberg, P. K. Shufflebotham, and K. C. Kao, J. Appl. Phys. **64**, 688 (1988).
[17] I. An, H. V. Nguyen, N. V. Nguyen, and R. W. Collins, Phys. Rev. Lett. **65**, 2274 (1990).
[18] S. Boultadakis, S. Logothetidis, and S. Ves, J. Appl. Phys. **72**, 3648 (1992).
[19] G. Kragler, H. Bender, G. Willeke, E. Bucher, and J. Vanhellemont, Appl. Phys. A: Solids Surf. **58**, 77 (1994).
[20] S. Adachi, T. Matsumura, and T. Suzuki, Jpn. J. Appl. Phys., Part 1 **33**, 1931 (1994).
[21] H. Shirai, B. Drévillon, and I. Shimizu, Jpn. J. Appl. Phys., Part 1 **33**, 5590 (1994).
[22] H. G. Tompkins and P. H. Williams, J. Vac. Sci. Technol. A **15**, 992 (1997).
[23] D. Ewald, M. Milleville, and G. Weiser, Philos. Mag. B **40**, 291 (1979).
[24] T. Haage, U. I. Schmidt, H. Fath, P. Hess, B. Schröder, and H. Oechsner, J. Appl. Phys. **76**, 4894 (1994).
[25] B. Drévillon, J. Perrin, J. M. Siefert, J. Huc, A. Lloret, G. de Rosny, and J. P. M. Schmitt, Appl. Phys. Lett. **42**, 801 (1983).
[26] I. An, Y. M. Li, C. R. Wronski, H. V. Nguyen, and R. W. Collins, Appl. Phys. Lett. **59**, 2543 (1991).
[27] G. Yu, T. Soga, C. L. Shao, T. Jimbo, and M. Umeno, Appl. Surf. Sci. **113/114**, 489 (1997).
[28] S. Adachi, Phys. Rev. B **38**, 12 966 (1988).
[29] T. Suzuki and S. Adachi, Jpn. J. Appl. Phys., Part 1 **32**, 4900 (1993).

[30] D. Y. Smith, in *Handbook of Optical Constants of Solids*, edited by E. D. Palik (Academic, Orlando, 1985), p. 35.
[31] D. E. Aspnes and A. A. Studna, Phys. Rev. B **27**, 985 (1983).
[32] S. Adachi, Phys. Rev. B **43**, 12 316 (1991).
[33] H. Mori and S. Adachi (unpublished).
[34] M. Fang and B. Drévillon, J. Appl. Phys. **70**, 4894 (1991).
[35] M. Fang and B. Drévillon, J. Appl. Phys. **71**, 1992 (1992).
[36] A. H. Jayatissa, T. Yamaguchi, and Y. Hatanaka, Semicond. Sci. Technol. **11**, 1882 (1996).
[37] G. E. Jellison, Jr. and F. A. Modine, Appl. Phys. Lett. **69**, 371 (1996); **69**, 2137(E) (1996).